Atomistic simulation of amorphous germanium and its solid phase epitaxial recrystallization

M. Posselt* and A. Gabriel
Forschungszentrum Dresden-Rossendorf, Institute of Ion Beam Physics and Materials Research, P.O. Box 510119, D-01314 Dresden, Germany

(Received 17 February 2009; revised manuscript received 11 May 2009; published 9 July 2009)

Amorphous Ge and its recrystallization are investigated by molecular-dynamics simulations using a Stillinger-Weber-type interatomic potential. Unlike previously used parametrizations of this potential the parameter set employed in this work yields a reasonable description of all condensed phases of Ge. The preparation of amorphous Ge is performed by cooling from the molten state. Structural and thermal properties of the amorphous phase such as the pair correlation function, the atomic density, as well as the melting temperature are calculated and a good agreement with experimental data is found. In order to obtain the initial atomic configuration for the simulation of recrystallization of amorphous Ge, a simulation cell that contains an amorphous and a crystalline layer is carefully prepared by melting a part of a primarily crystalline simulation cell and by cooling the liquid in a similar manner as in the preparation of bulk amorphous Ge. The recrystallization is simulated in the temperature range between 600 and 950 K. The simulation cell is built in such a manner that the main regrowth direction is parallel to [100]. Using an efficient characterization method the configuration of the current amorphous-crystalline interface, its average position with respect to the [100] direction, and its roughness given by the rms deviation of this position are determined throughout the simulations. Consistently with former models for Si it is found that recrystallization of amorphous Ge occurs mainly at small {111} facets and is characterized by a sequential local rearrangement of atomic bonds and positions. In very good agreement with experiments the dependence of the velocity of solid phase epitaxial recrystallization on temperature can be approximated by a straight line in an Arrhenius plot. However, the absolute value of the velocity is too high compared to the experimental data. The main reason for this discrepancy may be the overestimation of the flexibility of atomic bonds by the present interatomic potential which leads to an underestimation of the activation energy. Similar to the state of the art in atomistic simulations of solid phase epitaxial regrowth in Si, there is not yet a suitable interatomic potential which allows a consistent quantitative modeling of both the condensed phases and the solid phase epitaxial recrystallization.

DOI: 10.1103/PhysRevB.80.045202 PACS number(s): 81.10.Jt, 68.35.bj, 85.40.Ry, 61.43.Dq

I. INTRODUCTION

The renewed interest in Ge as a high mobility substrate has led to numerous investigations on shallow junction formation by ion beam processing (see, e.g., Refs. 1–3 and references therein). In order to achieve a substantial concentration of dopant atoms, they must be implanted at relatively high fluences which may lead to amorphization of the Ge substrate. On the other hand, an amorphous Ge layer may be also formed by preamorphization implantation with Ge ions. This processing step is often used before the implantation of dopants in order to avoid channeling effects and to enhance the electrical activation during postimplantation annealing.[1,3,4] In the first stage of annealing the amorphous Ge layer regrows by solid phase epitaxy. Experimental investigations showed that this process occurs in a similar manner as in Si. However, the effective activation energy is lower so that at a given temperature the regrowth of amorphous Ge is faster than that of amorphous Si.[5–12]

The main subject of the present work is the atomistic simulation of amorphous Ge and its recrystallization. Molecular-dynamics (MD) calculations using classical interatomic potentials are employed. This method is very well suited for the study of solid phase epitaxial recrystallization (SPER) under relatively realistic conditions, since it allows the consideration of several thousand atoms and/or a time scale up to several hundreds of nanoseconds. This is hardly possible if tight-binding MD or even MD simulations based on the density-functional theory (DFT) would be used because they are much more computationally intensive than classical MD simulations. While in the last decade several authors investigated SPER in Si,[13–17] the recrystallization of amorphous Ge layers has not yet been considered. The present paper is organized as follows. At first a Stillinger-Weber-type interatomic potential is introduced which is used in all investigations. The second part of the work deals with the preparation of amorphous Ge with realistic properties. The results of the MD simulations are compared to experimental data and results of previous theoretical investigations. In the third part of the paper a realistic atomic system containing an amorphous and a crystalline layer is prepared. Then, the system is heated to a given temperature and the recrystallization of the amorphous layer is monitored by different methods including visualization and statistical analysis. Regrowth velocities are calculated for a wide temperature range. The results are compared to experimental data from the literature. During the simulation of SPER the evolution of the roughness and the morphology of the amorphous-crystalline (a-c) interface are investigated.

II. INTERATOMIC POTENTIAL

In the literature several parametrizations of Stillinger-Weber-type potentials[18] for Ge can be found[19–28] whereas

TABLE I. Parameters of the Stillinger-Weber-type potential used in this work.

Scaling		Two-body part				Three-body part		Cutoff
ε (eV)	σ (Å)	A	B	p	q	λ	γ	a
1.93	2.181	7.049 556 277	0.602 224 558 4	4	0	19.5	1.19	1.8

only one parameter set exists for a Tersoff-type potential.[29] In this work a Stillinger-Weber-type potential shall be used. This potential consists of a two-body part V_2 and a three-body part V_3. The potential energy of an atomic system is given by

$$E_{\mathrm{pot}} = \sum_{\substack{i,j \\ i<j}} V_2(\mathbf{r}_i,\mathbf{r}_j) + \sum_{\substack{i,j,k \\ i<j<k}} V_3(\mathbf{r}_i,\mathbf{r}_j,\mathbf{r}_k).$$

The positions of atoms are denoted by $\mathbf{r}_i$, $\mathbf{r}_j$, and $\mathbf{r}_k$. The two-body part is given by

$$V_2(\mathbf{r}_i,\mathbf{r}_j) = \varepsilon f_2(r_{ij}/\sigma),$$

$$f_2(\tilde{r}) = \begin{cases} A(B\tilde{r}^{-p} - 1)\exp[(\tilde{r} - a)^{-1}], & \tilde{r} < a \\ 0, & \tilde{r} \geq a, \end{cases}$$

where ε and σ are the scaling parameters for energy and length, respectively. The quantity r_{ij} denotes the distance between atoms i and j, whereas $\tilde{r}$ is the atomic distance in units of σ. Furthermore, A, B, and p are the parameters of the two-body part and a is the cutoff of the two-body and the three-body parts. The following relations hold for the three-body part:

$$V_3(\mathbf{r}_i,\mathbf{r}_j,\mathbf{r}_k) = \varepsilon f_3(\mathbf{r}_i/\sigma,\mathbf{r}_j/\sigma,\mathbf{r}_k/\sigma),$$

$$f_3(\tilde{\mathbf{r}}_i,\tilde{\mathbf{r}}_j,\tilde{\mathbf{r}}_k) = h(\tilde{r}_{ij},\tilde{r}_{ik},\theta_{jik}) + h(\tilde{r}_{ji},\tilde{r}_{jk},\theta_{ijk}) + h(\tilde{r}_{ki},\tilde{r}_{kj},\theta_{ikj}),$$

$$h(\tilde{r}_{ij},\tilde{r}_{ik},\theta_{jik}) = \lambda \exp[\gamma(\tilde{r}_{ij} - a)^{-1} + \gamma(\tilde{r}_{ik} - a)^{-1}] \times \left(\cos\,\theta_{jik} + \frac{1}{3}\right)^2,$$

where θ_{jik} is the angle between $\mathbf{r}_{ij}$ and $\mathbf{r}_{ik}$, and λ and γ are the three-body parameters. With regard to essential properties of diamond-structure Ge the existing parameter sets for this potential can be divided in two classes. The first yields a correct cohesive energy but a melting temperature more than 1000 K above the experimental value (cf. Refs. 19 and 27), and the second gives an incorrect cohesive energy but the right melting point (cf. Ref. 27). In both cases the lattice constant is reproduced well. In the present work the values of Ding *et al.*[19] are used for the scaling parameters ε and σ as well as for the parameters of the two-body part of the potential A, B, and p, since they provide the experimental data for cohesive energy and lattice constant. The value for the cutoff a is also taken from Ref. 19. The values of the three-body parameters λ and γ are optimized under following conditions: (i) For diamond-structure Ge the elastic constants, the melting point, as well as the formation and migration energies of point defects are reproduced within certain limits. (ii) The energetics of other crystalline phases and the structure of the liquid are described reasonably well. The parameter set of the potential used in the present work is given in Table I. The structural and defect data calculated using this parametrization are given in Tables II–IV. Note that defect formation energy and formation volume were calculated using the method described in Ref. 30. The values obtained for the migration energy of the vacancy and the self-interstitial are 0.44 and 0.79 eV, respectively. The migration mechanisms of point defects in diamond-structure Ge are identical to those found in Ref. 30 for vacancies and self-interstitials in diamond-structure Si.

The following discussion is focused to investigations of the melting of diamond-structure Ge and of the structure of the liquid. Both issues are relevant for the preparation of amorphous Ge considered in Sec. III. Two alternative methods are used to investigate melting. In the first case the perfect crystal at 0 K is the starting point of $(N,P,H$ with $P=0)$ MD simulations, where N, H, and P are the total number of atoms, the total enthalpy, and the pressure, respectively. Heating is performed by the continuous but slow increase in the velocity of the atoms and zero pressure is maintained

TABLE II. Properties of diamond-structure Ge obtained by the Stillinger-Weber-type potential with parameters given in Table I. d: lattice constant; E_c: cohesive energy per atom; c_{11}, c_{12}, and c_{44}: (unrelaxed) elastic constants; T_m: melting point; ΔH_m: heat of fusion.

d (Å)	E_c (eV)	c_{11} (GPa)	c_{12} (GPa)	c_{44} (GPa)	T_m (K)	ΔH_m (eV)
5.654	−3.86	119	62.4	84.7	1360	0.249

TABLE III. Formation energy E_f and formation volume Ω_f of the vacancy and different self-interstitial configurations in diamond-structure Ge. The Stillinger-Weber-type potential with parameters given in Table I was used in the calculations. The hexagonal interstitial is not stable. Note that in the perfect crystal the volume per atom is about 22.77 Å^3.

Defect configuration	E_f (eV)	Ω_f (Å^3)
Tetrahedral vacancy	2.22	−25.5
Tetrahedral interstitial	3.98	19.6
⟨110⟩ dumbbell	3.59	7.47
Extended ⟨110⟩ dumbbell	3.01	1.42
⟨100⟩ dumbbell	4.55	1.42

TABLE IV. Properties of several lattice structures of Ge determined by the Stillinger-Weber-type potential with parameters given in Table I. DIA: diamond structure; SC: simple cubic; BCC: body-centered cubic; FCC: face-centered cubic; ΔE: energy difference with respect to diamond structure.

Lattice structure	d (Å)	E_c (eV)	ΔE (eV)
DIA (A4)	5.654	−3.86	0
SC (A_h)	2.709	−3.67	0.19
BCC (A2)	3.371	−3.66	0.20
FCC (A1)	4.306	−3.56	0.30

using a Berendsen barostat.[31] The most important result of these calculations are representations of the average potential energy per atom and the average atomic volume versus temperature as depicted in Figs. 1(a) and 1(b). These results were obtained for a cubic simulation cell consisting of 1000 atoms. The figures show a hysteresis which is typical for a first-order phase transition. The melting point and the heat of fusion obtained from these figures are 1360 K and 0.249 eV, respectively. Despite some differences this is in satisfactory agreement with the experimental values of 1210 K (Ref. 32) and 0.382 eV.[33,34] Like in the case of Si and water, melting of Ge leads to an anomalous increase in the density. This observation is confirmed by the simulations that provide a density increase of about 10%. It must be emphasized that the hysteresis method yields only reliable results for a sufficiently slow increase in the atomic velocities. Otherwise, superheating causes an overestimation of the melting temperature. In this work the atomic velocities were scaled at every 3 ps using different factors f_{scal} depending on the potential energy per atom E_c^A: $f_{\mathrm{scal}}=1.1$ for $E_c^A<-3.8$ eV and $E_c^A>-3.1$ eV; $f_{\mathrm{scal}}=1.05$ for $-3.8\ \mathrm{eV}\leq E_c^A<-3.7$ eV and $-3.2\ \mathrm{eV}\leq E_c^A<-3.1$ eV; $f_{\mathrm{scal}}=1.025$ for $-3.7\ \mathrm{eV}\leq E_c^A<-3.6$ eV and $-3.3\ \mathrm{eV}\leq E_c^A<-3.2$ eV; $f_{\mathrm{scal}}=1.0125$ for $-3.6\ \mathrm{eV}\leq E_c^A<-3.3$ eV. Larger cubic cells containing 4096 and 8000 atoms were also considered in the melting simulations. No systematic influence of the system size was found. The analysis of the results of the different simulations yields statistical errors of ±40 K and ±0.1 eV for the melting temperature and the heat of fusion, respectively. The second method considers the coexistence of the liquid and the solid phase using (N,V,E) MD simulations, where E and V are the total energy and the total volume, respectively. The coexistence states are determined by altering the volume of the whole simulation cell and by calculating the corresponding values of pressure and temperature.[35] The resulting representation $P(T)$ yields the melting point at $P=0$. Using the Clausius-Clapeyron equation the derivative $\frac{dP}{dT}$ at the melting point can be related to the melting temperature, the heat of fusion, and the difference between the atomic volumes in the solid and the liquid at the melting point. In this work the coexistence method was selectively used to check the accuracy of the procedure that considers the hysteresis during the phase transition. The simulation cell was a cuboid with the long side parallel to the [100] axis and containing 3000 atoms. A melting temperature of 1307 ± 15 K was obtained.

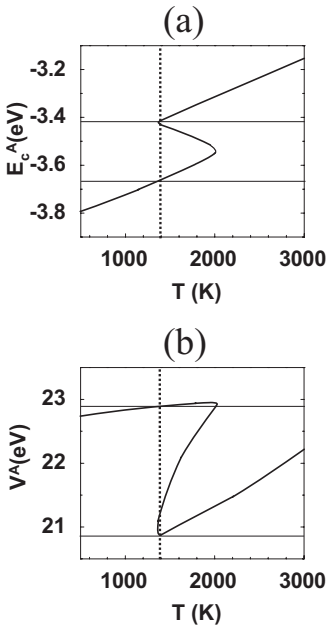

FIG. 1. Average potential energy E_c^A (a) and average volume V^A (b) per atom versus temperature. The thick lines are the result of smoothing the simulation data. The dotted and the thin solid lines illustrate how to determine the melting point, the heat of fusion, as well as the difference between the atomic volumes in the solid and the liquid at the melting point.

At the melting point the hysteresis method yields $\frac{dP}{dT}=-8.98\times10^{-5}$ eV Å^{-3} K^{-1} whereas the coexistence method gives $\frac{dP}{dT}=-8.91\times10^{-5}$ eV Å^{-3} K^{-1}. Therefore, the results obtained by both methods are rather similar.

Figure 2 shows the pair correlation function $g(r)$ and the static structure factor $S(k)$ of liquid Ge determined by the simulations in comparison with data measured by x-ray and neutron diffraction as well as by x-ray absorption spectroscopy.[36–39] Simulations and experiments were performed at or near the respective melting temperature. The overall agreement of calculated and measured data is good. However, the shoulder or hump to the right of the first peaks of $g(r)$ and $S(k)$ which arises from a residual covalent crystal-like arrangement of the atoms[38] is overestimated by the simulations. The simulation results for the atomic density and the coordination number at the melting point agree well with the corresponding experimental data.

III. PREPARATION OF AMORPHOUS Ge

The simulation cell is a cube consisting of 1000 atoms, with x, y, and z directions parallel to the [100], [010] and [001] axes, respectively. At the beginning of the simulation all atoms are arranged in a crystal with diamond structure. The dimensions of the cube are $5d\times5d\times5d$, where d is the lattice constant. Three-dimensional periodic boundary conditions and the isobaric-isothermal ensemble $(N,P,T$ with $P=0)$ are considered. The simulation cell is coupled to a Berendsen thermostat and a Berendsen barostat.[31] In the first simulation step liquid Ge is prepared by equilibrating the system at 2700 K for 100 ps. Then, the three-body parameter

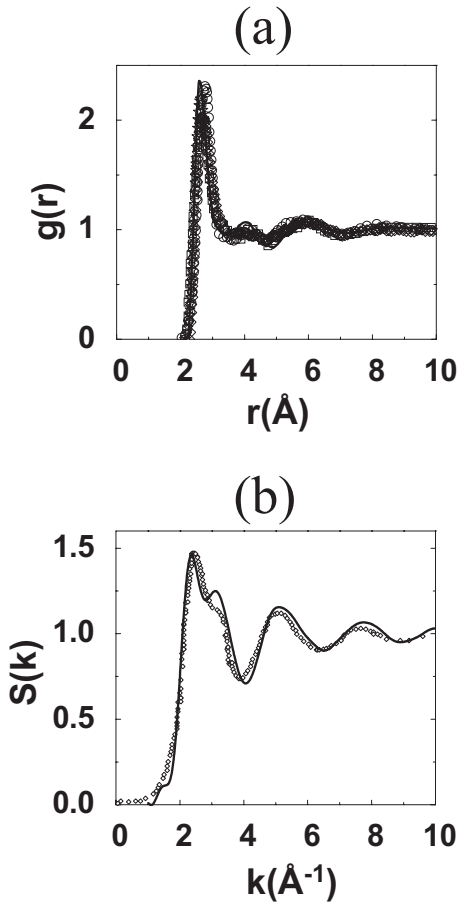

FIG. 2. Pair correlation function (a) and static structure factor (b) of liquid Ge determined by simulations (thick lines) in comparison with experimental data (symbols). The thick lines are the result of smoothing the simulation data. Neutron-diffraction results of Gabathuler *et al.* (Ref. 36) and Salmon (Ref. 37) are depicted by open squares and diamonds, respectively. Data obtained by x-ray diffraction (Ref. 38) and x-ray absorption spectroscopy (Ref. 39) are shown by open circles and asterisks, respectively. The latter data are only available in the range of the first peak and, therefore, the asterisks are hidden behind the other symbols.

λ of the interatomic potential is increased by a factor of 1.6, and a further equilibration is performed at 2700 K for 100 ps. In the next step the system is cooled down to 300 K at a cooling rate of 0.1 K ps^{-1}. Finally, the three-body parameter λ is decreased to its original value and the system is equilibrated at 300 K for 100 ps. It must be emphasized that the above procedure does not correspond to a real cooling process. However, in the following it will be shown that the present method yields amorphous Ge with realistic properties. On the other hand, in experiments amorphous Ge is not produced by cooling from the melt but by other methods such as ion implantation and sputter deposition. The preparation of amorphous Ge as described above corresponds to the method suggested by Luedtke *et al.*[40] in order to simulate amorphous silicon. The temporary increase in the three-body parameter λ leads to an additional preference for the tetrahedral coordination. The values for the temporary increase in the three-body parameter λ and for the cooling rate used in present investigations are the result of an optimization with respect to the properties of amorphous Ge. It should be mentioned that it was not possible to prepare amorphous Ge with realistic properties performing only a very slow cooling from the melt. However, in these investigations the cooling rate was varied just by 4 orders of magnitude since the computational effort rises dramatically for slower cooling rates.

The structural properties of amorphous Ge prepared by the method described above are presented in Table V and in Fig. 3. The comparison with experimental data[41–47] for amorphous Ge layers produced by different methods shows a generally good agreement. In particular the atomic density and the coordination number determined by simulations agree well with those of the samples prepared by ion implantation or by evaporation followed by ion implantation. On the other hand, sputtering and evaporation lead to samples with lower atomic density and coordination which may be due to void formation during deposition. The pair correlation function $g(r)$ and the static structure factor $S(k)$ obtained by the simulations are very similar to the experimental data determined by x-ray, neutron, or electron diffraction (Fig. 3). Furthermore, a good agreement between simulations and experimental data is found for the average bond length, the average bond angle, as well as for the root-mean-square (rms) deviations of these quantities (Table V). At 300 K simulations yield a difference of 0.144 eV between the cohesive energy per atom in amorphous and in diamond-structure Ge. This is somewhat higher than the experimental value of 0.120 eV for the heat of crystallization of amorphous Ge.[33] The thermal stability of the amorphous Ge prepared by the simulations was tested by reheating to 900 K and subsequent cooling to 300 K. The structural properties obtained after this treatment are almost identical to those of the originally prepared amorphous Ge. This demonstrates that the preparation procedure described above yields fully relaxed material.

The melting of amorphous Ge was simulated in the same manner as the melting of diamond-structure Ge. In agreement with experiments a first-order phase transition was found but the hysteresis is much less pronounced than in the case of melting crystalline Ge. The melting point of 1024 K determined by the simulations is close to the value of 965 K which was estimated using experimental data of other thermodynamic quantities.[33,48] On the other hand, the calculated heat of fusion of 0.0726 eV/atom is less than the experimental value of 0.269 eV/atom.[49,50] In Sec. II a similar difference has been also found for the heat of fusion of diamond-structure Ge. In qualitative agreement with measurements, melting of amorphous Ge leads to an anomalous increase in the atomic density by about 11%.

The few previous attempts to simulate amorphous Ge considered cooling from the melt at a constant atomic density given by the experimental value. The only exception is the work of Bording[51] who considered the isobaric-isothermal ensemble ($P=0$) and the Tersoff[29] potential. He obtained realistic values for most structural properties of amorphous Ge. Similar results were obtained using a Stillinger-Weber-type potential.[19] However, both the Tersoff potential and the potential used in Ref. 19 yield melting points for diamond-structure and amorphous Ge which are far above the experimental values. Therefore, these potentials are not suitable for the simulation of SPER. MD simu-

TABLE V. Structural properties of amorphous Ge at 300 K: comparison between results of present atomistic simulations with experimental data and previous theoretical results (n: atomic density; N: coordination number; R_b: average bond length; ΔR_b: rms deviation of bond length; θ: average bond angle; $\Delta\theta$: rms deviation of bond angle). In this work the coordination number was determined assuming a cutoff distance of 3.03 Å (cf. Fig. 3).

	n (Å^{-3})	N	R_b (Å)	ΔR_b (Å)	θ (deg)	$\Delta\theta$ (deg)
This work	0.0434	4.03	2.48	0.081	108.9	11.08
Experimental results—preparation method/ analysis						
Ion implantation at RT/surface profilometry and Rutherford backscattering spectrometry in channeling direction (Ref. 41)	0.0435					
Evaporation/x-ray diffraction (Ref. 42)	0.0375	3.3				
Evaporation followed by ion implantation/x-ray diffraction (Ref. 42)	0.042	3.95				
Sputtering at 150 °C/x-ray diffraction (Ref. 43)	0.0406	3.79	2.47	0.087	109.5	10
Sputtering at 350 °C/x-ray diffraction (Ref. 43)	0.0428	3.91	2.47	0.089	109.5	10
Sputtering at −20 °C/x-ray diffraction (Ref. 44)	0.0397	3.85	2.46	0.085	109	10
Electron beam evaporation at 100 °C/neutron diffraction (Ref. 45)	0.0398	3.68	2.463	0.074	108.5	9.7
Ion implantation at RT/x-ray absorption fine-structure spectroscopy (Ref. 46)		3.94	2.461–2.464			
Previous theoretical results—method						
Classical MD, Tersoff (Ref. 29) potential, $P=0$, results for 0 K (Ref. 51)	0.0430	4.1	2.49			
Classical MD, Stillinger-Weber-type potential, n =const (Ref. 19)		4.01	2.48			
Cooling from the melt, DFT-MD, n=const (Ref. 52)		4.04	2.48	0.1	107.7	17.9
Cooling from the melt, DFT-MD, n=const (Ref. 53)		4.18				

lations based on the DFT also led to reasonable properties of amorphous Ge.[52,53] However, because of the computational costs this type of simulations cannot be used to investigate SPER.

IV. PREPARATION OF A SYSTEM CONTAINING AN AMORPHOUS AND A CRYSTALLINE LAYER

The simulation cell is chosen as cuboid with the long side parallel to [100] (x axis) and the short sides parallel to [010] and [001]. Initially the atomic arrangement corresponds to the diamond structure. In the present work a smaller cell with 3000 atoms and the dimensions $15d\times5d\times5d$ as well as a larger cell with 54 000 atoms and the dimensions $30d\times15d\times15d$ are considered. Three-dimensional periodic boundary conditions are used. The simulation cell is subdivided along the x axis: the inner part extends from $-0.5fL_x$ to $+0.5fL_x$, where L_x is equal to $15d$ or $30d$, with $f=0.8$. The two parts are coupled to different Berendsen thermostats, and zero pressure is maintained at the cell boundaries at $-L_x$ and $+L_x$ using a Berendsen barostat. In the first simulation step the inner and outer parts are equilibrated at 2700 and 300 K, respectively, for 100 ps. The inner part becomes liquid whereas the two outer parts remain crystalline. Then, in the whole simulation cell the three-body parameter λ of the interatomic potential is increased by a factor of 1.6, and a further equilibration is performed for 100 ps, at the same temperatures as in the first step. In the third step the inner part is cooled from 2700 to 300 K at a cooling rate of 1 K ps^{-1} whereas the temperature of the outer part is maintained at 300 K. Finally, the three-body parameter λ of the interatomic potential is reset to its original value and the whole system is equilibrated at 300 K for 300 ps. As the result of the whole preparation procedure the inner and the outer parts of the simulation cell consist of amorphous and crystalline Ge, respectively. This system mimics the real situation with an amorphous surface layer and a single-crystalline substrate. It is therefore well suited to be used as initial configuration in the simulation of the recrystallization of the amorphous layer. The preparation method described above is similar to that employed in Sec. III to produce bulk amorphous Ge. The values used for the parameter f, for the temporary increase in the three-body parameter λ, and for the cooling rate are the result of an optimization under the following conditions: (i) amorphous and crystalline Ge

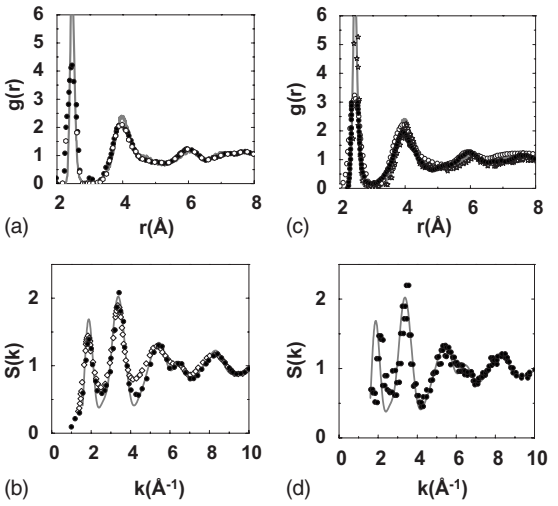

FIG. 3. Pair correlation function and static structure factor of amorphous Ge obtained in this work (thick gray lines) in comparison with experimental data and results of previous calculations (symbols): (a) Results of neutron diffraction (Ref. 45) (full circles) and x-ray diffraction (Ref. 43) (open circles). (b) Data obtained by electron diffraction (Ref. 47) (open diamonds) and neutron diffraction (Ref. 45) (full circles). (c) Results of calculations using a Stillinger-Weber-type potential (Ref. 19) (open circles), the Tersoff (Ref. 29) potential (Ref. 51) (open asterisks), and DFT (Ref. 52) (full circles). (d) Results of DFT calculations (Ref. 52) (full circles).

should form well separated layers. (ii) The structural properties of both phases should be almost identical to those of the corresponding bulk amorphous and crystalline material. Both conditions imply that recrystallization of the liquid phase must be suppressed during the cooling process.

In order to distinguish atoms of the crystalline part from atoms of the amorphous part the following characterization method is applied to the configuration obtained as the results of the above preparation procedure. During an additional equilibration step at 300 K time averages of the atomic coordinates are calculated over a period $\Delta t_{\mathrm{av}}=2$ ps. From these data the bond angles are obtained for the averaged system. The time average eliminates the thermal vibrations of the atoms in the crystalline state and reveals its inherent structure.[54] Such a structure can be also determined by quenching the system to 0 K. The inherent structure shows a much narrower bond angle distribution than the instantaneous structure at a given temperature. On the other hand, in the amorphous state the disorder is not due to thermal vibrations but due to the amorphous structure itself. Therefore, the time average does not change the bond angle distribution in this case. Based on time averages of the atomic coordinates the following criteria are used to assign an atom to the crystalline part: (i) the atom has four nearest neighbors within the cutoff distance of 3.03 Å. (ii) The maximum deviation of the cosine of all bond angles from the ideal value $-\frac{1}{3}$ defined by the diamond structure must not exceed a threshold $\Delta \cos_{\mathrm{th}}=0.15$. (iii) Two or more nearest neighbors of the atom belong to the crystalline part. (iv) Three or more second nearest neighbors belong to the crystalline part. Note that the values of Δt_{av} and $\Delta \cos_{\mathrm{th}}$ as well as for the cutoff distance are the result of several attempts aimed at an optimal characterization.

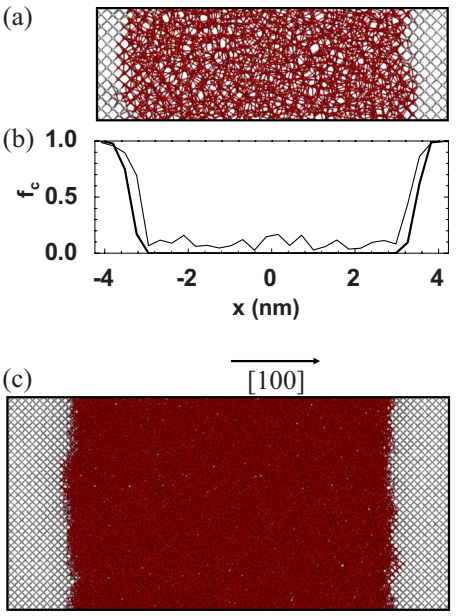

FIG. 4. (Color online) Initial atomic configurations used in Sec. V in the simulation of the recrystallization of the amorphous layer. The smaller system consists of 3000 atoms (a), whereas the larger system contains 54 000 atoms (c). The spheres depict the positions of atoms time-averaged over 2 ps at a temperature of 300 K. The figure demonstrates the ability of the characterization procedure based on the criteria (i)–(iv) (see text) to distinguish between atoms in the amorphous and the crystalline part which are shown by red and gray color (gray scale: dark and light gray), respectively. For the smaller system the distribution of the crystalline fraction f_c along the x axis is also shown (b). Two alternative methods to determine whether an atom belongs to the crystalline or amorphous part were applied: criteria (i)–(iv) (see text) and the structure factor $s(x)$. The results of the first and the second method are depicted by thick and thin lines, respectively.

An alternative but less consistent method to determine whether an atom belongs to the crystalline or the amorphous part is based on the consideration of the structure factor[16]

$$s(x)=\frac{1}{N_x}\left|\sum_{x<x_i<x+\Delta x}\exp(i\mathbf{k}\mathbf{r}_i)\right|.$$

The quantity $\mathbf{k}$ is a vector of the reciprocal lattice parallel to the x axis, $\mathbf{k}=\frac{8\pi}{d}\mathbf{e}_x$, $\mathbf{e}_x$ being the unit vector along the x axis. N_x denotes the number of atoms in a crystalline layer perpendicular to the x axis and the sum is over all atoms i having time-averaged coordinates $\mathbf{r}_i$ and $x_i=\mathbf{r}_i\mathbf{e}_x$ between x and $x+\Delta x$. In the present work $\Delta x=\frac{1}{2}d$ is used. The structure factor $s(x)$ is equal to 1 and around 0 if the depth interval belongs to the crystalline and the amorphous part, respectively. In this manner it is possible to determine the ratio of the number of atoms in the crystalline part to the total number of atoms in dependence on x. This ratio is called crystalline fraction. It should be noticed that the characterization via $s(x)$ becomes incorrect if stacking faults are formed during recrystallization.

Figures 4(a) and 4(c) illustrate the atomic configurations

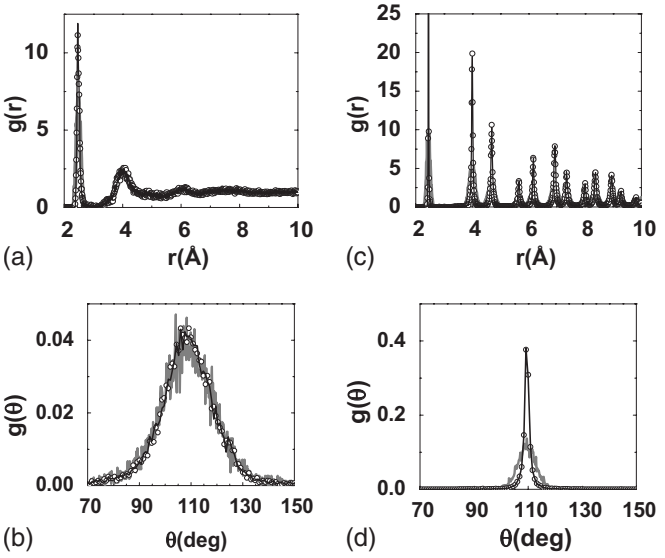

FIG. 5. Pair correlation function $g(r)$ and bond angle distribution $g(\theta)$ inside the amorphous [(a) and (b)] and the crystalline part [(c) and (d)] of the time-averaged atomic configuration displayed in Fig. 4(a) (black lines). These characteristics are also shown for a snapshot of the same atomic configuration at 300 K (thick gray lines) and for the inherent structure obtained by quenching from 300 to 0 K (open circles).

obtained as the result of the preparation procedure described above. The inherent structure determined by time averaging over 2 ps is shown. Well separated amorphous and crystalline layers are found. The simulation cell comprises about 80% amorphous and 20% crystalline material. The figure demonstrates the ability of the characterization procedure based on the criteria (i)–(iv) (see above) to distinguish between atoms of the crystalline and the amorphous material. The two systems shown in Fig. 4 are used as start configurations in the simulation of the recrystallization process in Sec. V. Figure 4(b) depicts the crystalline fraction in dependence on the x coordinate for the system given in Fig. 4(a). The two alternative methods to determine whether an atom belongs to the crystalline or amorphous part yield very similar results. Therefore, only the first procedure is used in the following. The pair correlation function and the bond angle distribution for the amorphous and crystalline part of Fig. 4(a) are displayed in Fig. 5. These characteristics are shown for the instantaneous and the inherent structures. Figure 6 demonstrates that the pair correlation functions and the bond angle distributions for the amorphous and crystalline part of Fig. 4(a) agree well with the corresponding characteristics in bulk amorphous or crystalline material. Note that this figure depicts the results for the inherent structures obtained by time averaging. The data for bulk material were determined considering a system containing 1000 atoms (cf. Sec. III). The peaks of the distributions for the crystalline part are less pronounced than those for the bulk crystal. This is due to distortions of the crystalline material near the a-c interface. The difference would be smaller if the extension of the crystalline part along the x axis was larger.

The present method to prepare the initial configuration for simulating SPER is more advantageous than gluing a simulation cell containing amorphous material onto a crystalline substrate. This procedure was often used to prepare the initial configuration for the simulation of SPER in Si.[13,14,16,17] By gluing the two systems defects are generated at the interface which can be hardly removed, especially if recrystallization at relatively low temperatures is considered.[13] During the preparation used in this work the two a-c interfaces are formed in a less artificial manner. Compared to a simulation cell with an amorphous surface layer and a bottom crystalline layer[15,17] the present configuration has two advantages. Since the simulation cell is always very small in comparison to a real sample, the simulation of the recrystallization process would be influenced by the presence of a free surface. On the other hand, this influence does not play an important role during SPER in the real sample. Moreover, the present configuration contains two a-c interfaces. This allows an averaging over statistical fluctuations and the determination of a mean regrowth rate.

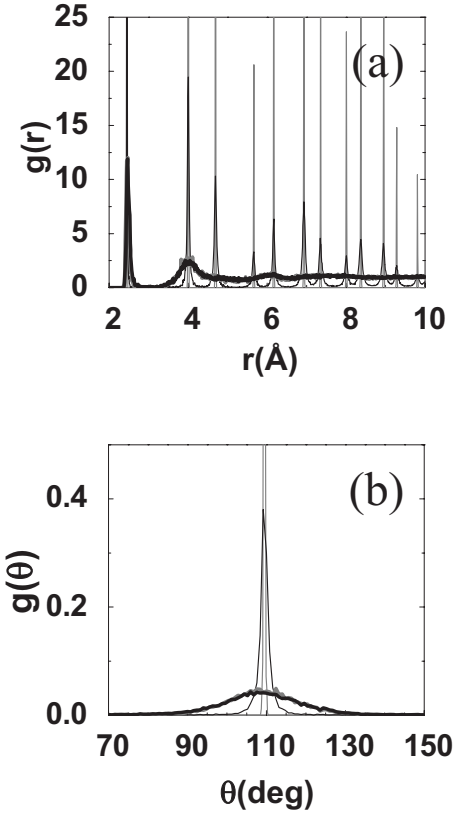

FIG. 6. Comparison of the pair correlation function (a) and the bond angle distribution (b) obtained for the amorphous and the crystalline part of the time-averaged atomic configuration shown in Fig. 4(a) (black lines) to corresponding characteristics of bulk amorphous and crystalline material (gray lines). The thick and thin lines show the data for the amorphous and crystalline case, respectively.

V. SOLID PHASE EPITAXIAL RECRYSTALLIZATION

The simulation of recrystallization of amorphous Ge is performed using the two systems shown in Fig. 4 as start configurations. In most simulations the smaller system is

TABLE VI. Overview of recrystallization simulations.

Simulation cell	Heating rate (K ps^{-1})	Temperature (K)	Simulation time (ns)
$15d \times 5d \times 5d$, 3000 atoms	1, 10	600	250
	1, 10	650	200
	1, 10, 20, 50, 100	700	40
	1, 10, 20, 50, 100	750	16
	1, 10, 20, 50, 100	800	5
	1, 10, 20, 50, 100	850	1.5
	1, 10, 20, 50, 100	900	1
	1, 10, 20, 50, 100	950	0.8
$30d \times 15d \times 15d$, 54000 atoms	10	700	20
	10	750	9
	10	800	8
	10	850	3
	10	900	2

considered. Due to the remarkably higher computational cost the larger system is only examined in selected cases for comparison. The whole simulation cell is coupled to a Berendsen thermostat and zero pressure is maintained at the cell boundaries at $-L_x$ and $+L_x$ using a Berendsen barostat. Before the simulation of recrystallization the temperature of the system must be increased from 300 K to the temperature at which the regrowth is to be investigated. The heating is carried out at different rates ranging from 1 to 100 K ps^{-1}. The simulation of recrystallization is performed at temperatures between 600 and 950 K. At the lower temperatures the required simulation time is much longer than at the higher temperatures. Table VI gives an overview of the calculations performed. The pair correlation function and the bond angle distribution of the amorphous and the crystalline part of the simulation cell are determined for each regrowth temperature. In all cases the characteristic properties of the two phases are found. During the simulation of recrystallization melting of the amorphous material[17] is never found. Throughout the simulation the characterization method based on time-averaged atomic coordinates and the criteria (i)–(iv) (cf. Sec. IV) is continuously applied in order to distinguish between atoms belonging to the crystalline and the amorphous part and to determine the current crystalline fraction as well as the current configuration of the a-c interface. The latter is obtained in the following manner: an atom is situated at the interface if it belongs to the crystalline part and if it has at least one nearest neighbor belonging to the amorphous part. Using the data on the current a-c interface its average position with respect to the x axis and its roughness given by the rms deviation of this position is calculated throughout the simulation of recrystallization. Since the simulation cell contains two interfaces an additional averaging of the results is performed. It should be noticed that the procedure to calculate the average position of the a-c interface with respect to the x axis and its rms deviation does only work properly if the amorphous part is contiguous and if the positions of the left and the right interfaces are at $x \leq 0$ and $x > 0$, respectively.

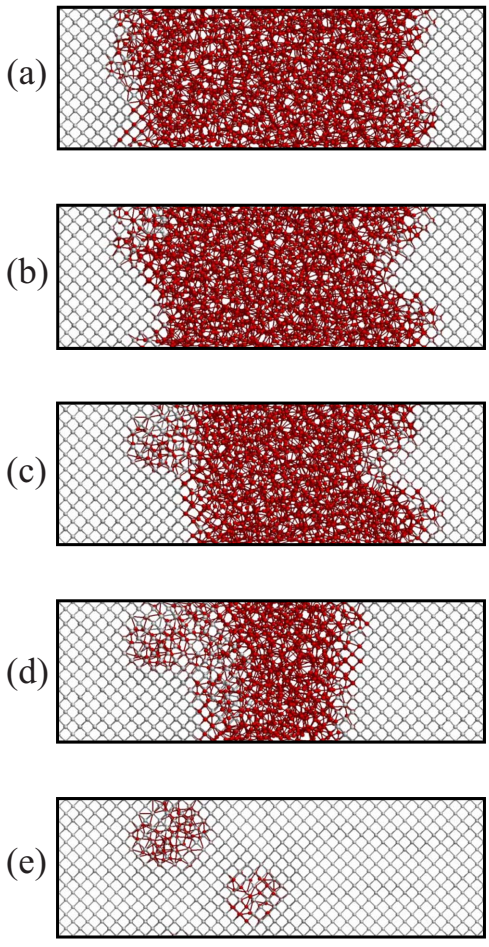

FIG. 7. (Color online) Recrystallization of the amorphous Ge layer at 800 K: after (a) 1 ns, (b) 2 ns, (c) 3 ns, (d) 4 ns, and (e) 5 ns. The simulation cell contains 3000 atoms. For details of the presentation see Fig. 4. Note that atoms that belong to defects formed by stacking faults are also shown by red color (gray scale: dark gray).

Figure 7 illustrates the recrystallization of amorphous Ge at 800 K. Two stages are found. The initial stage [Figs. 7(a)–7(c)] corresponds to the SPER process. Here, the amorphous part is contiguous and its thickness is large enough so that the two interfaces do not influence each other. In the final stage [Figs. 7(d) and 7(e)] the amorphous region becomes thinner and, eventually, isolated amorphous regions may exist and recrystallize independently of each other. This may lead to the generation of {111} stacking faults and defects as shown in Fig. 7(e). However, the occurrence of {111} stacking faults may be overestimated by present simulations since the Stillinger-Weber-type potential used does not penalize the formation of this type of stacking faults since the corresponding stacking fault energy is zero. Atomic mechanisms of regrowth are illustrated in Fig. 8. The a-c interface contains small {111} facets where recrystallization mainly takes place. This process is characterized by a sequential local rearrangement of atomic bonds and positions. In the well-known model for SPER in Si (Refs. 55 and 56) two stages are assumed: (i) kink formation at {111} terraces and (ii) kink propagation along ⟨110⟩ ledges on these terraces. The second stage is similar to the rearrangement process described above. However, using present simulation results it was not possible to find kink formation. This might be due to fact that the complexity of the atomic rearrangements hinders a proper identification of the formation of the kinks. {111} facets and complex interface structures containing these facets were also observed in atomistic simulations and experiments on SPER in Si.[14–16,57]

Figure 9 depicts the shift of the average position of the a-c interface with respect to the x axis versus time for the example of recrystallization at 800 K. As described above, these data are continuously produced during the simulation. The differences between the data obtained for the various velocities of heating the system from 300 to 800 K are due to statistical fluctuations. In order to determine the velocity of SPER a linear fit is performed to the curves depicting the shift of the a-c interface versus time. In the case of recrystallization simulation in the smaller cell containing 3000 atoms only the first 1 nm of the interface shift is included in the fit, since at the later stage of regrowth the amorphous layer is relatively thin and the two interfaces may influence each other. If the larger system with 54 000 atoms is considered the linear fit is performed up to a shift of 2 nm. At a given temperature the mean velocity of SPER is obtained by averaging over the corresponding velocities obtained for samples with various heating rates. At high temperatures the regrowth proceeds continuously and the shift of the a-c interface depends nearly linearly on time [Fig. 10(a)]. On the other hand, at low temperatures a discontinuous and rather nonlinear regrowth is found [Fig. 10(b)]. In this case the role of thermal fluctuations is more obvious than at high temperatures where they act more frequently and lead to a smoother regrowth. The development of the roughness of the a-c interface expressed by the rms deviation of the average position of the interface with respect to the x axis is shown in Figs. 10(c) and 10(d). At 900 K a nearly stationary value of about 0.21 nm is reached during the SPER stage of recrystallization. The value for 650 K is only 5% lower. The difference may be due to statistical fluctuations.

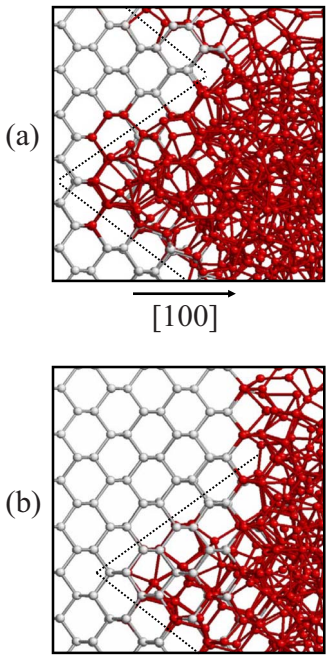

FIG. 8. (Color online) Recrystallization of a faceted interface: the upper and lower figures show a part of the a-c interface at 2 and 2.5 ns after the start of recrystallization, respectively, at 800 K. {111} planes containing facets and lying perpendicular to the {110} plane of the figures are marked by dotted lines.

The finite dimension of the simulation cell may cause the suppression or the preference of certain regrowth modes which are mainly determined by the boundary conditions perpendicular to the main recrystallization direction. Results obtained for the smaller and the larger cells are presented in Fig. 11. In the latter case the velocity of SPER is somewhat larger than in the former. Such a small difference is observed at all temperatures considered in the simulations. One cause may be the preference for different regrowth modes in the smaller and the larger cell. Another reason may be the fact that in the larger cell no stationary value of the interface roughness is reached during SPER simulation. However, it is

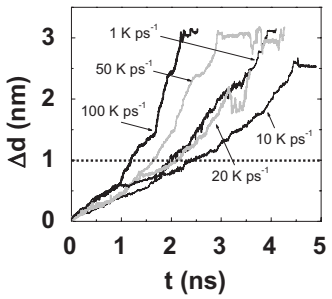

FIG. 9. Shift Δd of the average position of the a-c interface with respect to the [100] direction versus time t for the example of recrystallization at 800 K. Curves are shown for different velocities of heating the system from 300 to 800 K before the recrystallization simulation. The velocity of SPER is obtained by a linear fit to the curves within the first 1 nm of the interface shift. This region is marked by the dotted line. The results were obtained for the simulation cell consisting of 3000 atoms.

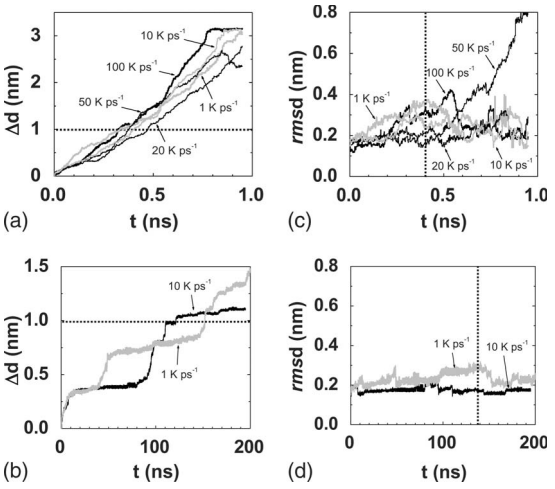

FIG. 10. Recrystallization versus time: shift of the average position of the a-c interface with respect to the x axis at 900 K (a) and 650 K (b) as well as the rms deviation of the average position of the interface with respect to the [100] at 900 K (c) and 650 K (d). For more details see Fig. 9.

also possible that the difference is simply due to statistical fluctuations.

Additional simulations were performed in order to investigate the influence of the conditions set by the barostat. Zero pressure is maintained not only at $-L_x$ and $+L_x$ but at all boundaries. Therefore, in contrast to the simulations discussed up to now, the extensions of the simulation cell in the [010] and [001] directions are not fixed to a value related to the lattice constant d (cf. Sec. IV) but are dependent on the

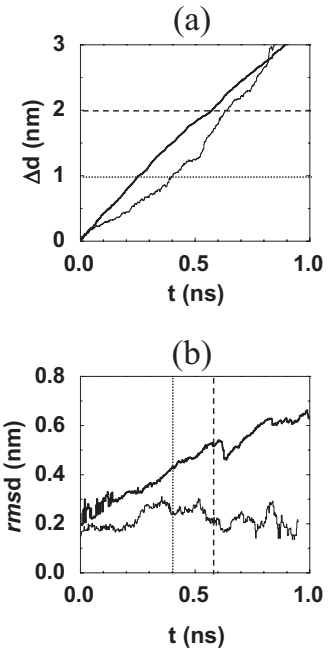

FIG. 11. Results obtained for the smaller (thin lines) and the larger cell (thick lines) at 900 K. In the case of the smaller and the larger cell the velocity of SPER is determined within the first 1 nm (dotted line) and 2 nm (dashed line) of the interface shift, respectively.

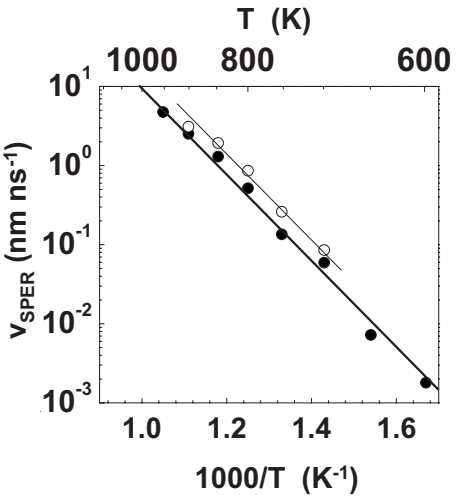

FIG. 12. Velocities of SPER obtained by the simulations in an Arrhenius plot. Results for the smaller and the larger system are depicted by full and open symbols, respectively.

recrystallization temperature. The smaller simulation cell consisting of 3000 atoms was considered. Various temperatures and samples that were heated to the given regrowth temperature at different rates were studied. The results are very similar to those presented above for a simulation cell with zero pressure maintained at the boundaries $-L_x$ and $+L_x$. There are only small differences due to statistical fluctuations but no systematic deviation is found.

Figure 12 shows the velocities of SPER obtained by simulations at different temperatures in an Arrhenius plot. In excellent agreement with experiments the theoretical results can be approximated by a straight line. In the case of the smaller system containing 3000 atoms the effective activation energy of SPER and the pre-exponential factor are 1.09 eV and 3.21×10^6 nm ns^{-1}, respectively. For the larger system with 54 000 atoms the estimated values are 1.09 eV and 5.55×10^6 nm ns^{-1}. The possible reasons for the difference between the results obtained for the smaller and the larger system have been already discussed above. The value of the effective activation energy cannot be simply related to formation or migration energies of the point defects (cf. Sec. II), or to the sum of point defect formation and migration energies. Doubt is cast on the idea that SPER occurs through a single thermally activated process. Instead several complex atomic rearrangement processes such as the bond switching at {111} facets described above contribute to the effective activation energy of SPER.[12,13]

The measured velocities of SPER are much lower than the values determined by the present simulations.[5–12] Most recent and very detailed experiments[12] yielded an activation energy of 2.15 eV and a pre-exponential factor of 2.6×10^7 nm ns^{-1}. The main reason for this large discrepancy between simulations and experiment may be the quality of the interatomic potential used in the calculations. Although this potential allows the simulation of crystalline, amorphous, and liquid Ge with realistic properties it does not describe SPER quantitatively correct. The activation energy of SPER may be related to the flexibility of the atomic bonds at the a-c interface. Obviously, the interatomic potential used

leads to an overestimation of this flexibility and, consequently, to an underestimation of the activation energy. The flexibility of bonds may be decreased by increasing the three-body parameter λ of the potential. However, this would increase the melting temperature both for amorphous and crystalline Ge which is predicted properly by the interatomic potential used in this work. Therefore, such a modification of the potential would not lead to a physically consistent modeling of recrystallization. A similar case was discussed by Krzeminski *et al.*[17] These authors simulated SPER in Si using several interatomic potentials and found that most potentials lead to regrowth velocities that are much higher than the measured data. Apparently, a good agreement with the experiments was obtained using the Tersoff potential.[58] However, the melting temperatures of amorphous and crystalline Si obtained by this potential are 600–800 K higher than the experimental values. If the temperature is rescaled using the ratio of the melting temperatures determined by experiment and simulation, the velocity of SPER determined using the Tersoff potential becomes also much higher than the measured data. This demonstrates that the use of the Tersoff potential does not result in a physically based improvement in the modeling of recrystallization. Until now it has not been possible to find a suitable interatomic potential for Si which allows both the correct prediction of the melting temperatures and the precise simulation of the SPER velocity.[13–17] Obviously, the same situation exists in the case of Ge.

VI. SUMMARY

Comprehensive atomistic simulations of amorphous germanium and its solid phase epitaxial recrystallization have been performed using a Stillinger-Weber-type interatomic potential. Contrary to previously used parametrizations of this potential the parameter set employed in this work yields a reasonable description of all condensed phases which are observed at zero pressure, i.e., diamond-structure, amorphous, and liquid Ge. The preparation of amorphous Ge has been performed by cooling from the melt using a method similar to that employed in the simulation of amorphous Si. The pair correlation function, the atomic density, the coordination number, the average bond angle, the melting temperature, and other structural and thermal properties have been calculated. The results of simulation are in good agreement with experimental data.

An atomic system that contains an amorphous and a crystalline layer has been prepared by melting a part of an initially crystalline simulation cell and by cooling the liquid in a similar manner as in the preparation of bulk amorphous Ge. This system is employed as initial configuration in the simulation of the recrystallization of amorphous Ge. The simulation cell is built in such a manner that the main direction of regrowth is parallel to [100]. An efficient characterization method to distinguish atoms of the crystalline part from atoms of the amorphous part uses time-averaged atomic coordinates and criteria concerning the atomic coordination, the bond angles, as well as the first and the second neighbor atoms in the averaged system. The present procedure to prepare the initial state for simulating the recrystallization of amorphous Ge leads to a more realistic system than methods previously used in the simulation of SPER in Si.

The recrystallization has been simulated in the temperature range between 600 and 950 K and over 0.8–250 ns. The configuration of the current a-c interface, its average position with respect to the [100] direction, and its roughness given by the rms deviation of this position have been continuously determined during the simulation. The recrystallization process consists of two stages. The first stage corresponds to SPER whereas in the second stage the amorphous region becomes thinner and, finally, isolated amorphous regions may recrystallize independently of each other. This may cause the generation of stacking faults and defects. The velocity of SPER has been obtained from a linear fit to the initial part of the curves depicting the shift of the a-c interface versus the simulation time. The velocity of SPER in the smaller simulation cell containing 3000 atoms is somewhat smaller than in the larger system with 54 000 atoms. This may be due to the fact that the finite cell dimensions may cause the suppression or the preference of certain regrowth modes which are determined by the boundary conditions perpendicular to the main recrystallization direction. The recrystallization has been found to take place mainly at small {111} facets. This process is characterized by a sequential local rearrangement of atomic bonds and positions. The dependence of the velocity of SPER on temperature can be approximated by a straight line in an Arrhenius plot. This agrees very well with the experimental results. However, the velocity of SPER determined by the simulations is too high compared to measured data. The main reason for this discrepancy may be the quality of the interatomic potential used. Obviously, the potential overestimates the flexibility of atomic bonds and, consequently, underestimates the activation energy of SPER. Similar to the state of the art in the atomistic simulation of SPER in Si it has not yet been possible to find an appropriate interatomic potential which allows both the reasonable prediction of the structural and thermal properties of the condensed phases and a quantitatively correct calculation of the SPER velocity. This important aspect should be taken into account in future efforts on the improvement of the interatomic potential.

*Corresponding author; m.posselt@fzd.de; FAX: +49 351 260 3285.

[1] E. Simoen, A. Satta, A. D'Amore, T. Janssens, T. Clarysse, K. Martens, B. De Jaeger, A. Benedetti, I. Hoflijk, B. Brijs, M. Meuris, and W. Vandervorst, Mater. Sci. Semicond. Process. **9**, 634 (2006).

[2] A. Satta, T. Janssens, T. Clarysse, E. Simoen, M. Meuris, A. Benedetti, I. Hoflijk, B. De Jaeger, C. Demeurisse, and W. Vand-

ervorst, J. Vac. Sci. Technol. B **24**, 494 (2006).
[3] M. Posselt, B. Schmidt, W. Anwand, R. Grötzschel, V. Heera, A. Mücklich, C. Wündisch, W. Skorupa, H. Hortenbach, S. Gennaro, M. Bersani, D. Giubertoni, A. Möller, and H. Bracht, J. Vac. Sci. Technol. B **26**, 430 (2008).
[4] A. Satta, E. Simoen, T. Clarysse, T. Janssens, A. Benedetti, B. De Jaeger, M. Meuris, and W. Vandervorst, Appl. Phys. Lett. **87**, 172109 (2005).
[5] L. Csepregi, R. P. Küllen, J. W. Mayer, and T. W. Sigmon, Solid State Commun. **21**, 1019 (1977).
[6] G. Q. Lu, E. Nygren, M. J. Aziz, D. Turnbull, and C. W. White, Appl. Phys. Lett. **56**, 137 (1990).
[7] G. Q. Lu, E. Nygren, and M. J. Aziz, J. Appl. Phys. **70**, 5323 (1991).
[8] G. Olson and J. Roth, in *Handbook of Crystal Growth*, edited by D. Hurle (Elsevier, New York, 1994), Vol. 3, Chap. 7, pp. 255–312.
[9] P. Kringhoj and R. G. Elliman, Phys. Rev. Lett. **73**, 858 (1994).
[10] T. E. Haynes, M. J. Antonell, C. A. Lee, and K. S. Jones, Phys. Rev. B **51**, 7762 (1995).
[11] S. Koffel, P. Scheiblin, and A. Claverie, ECS Trans. **16**, 229 (2008).
[12] B. C. Johnson, P. Gortmaker, and J. C. McCallum, Phys. Rev. B **77**, 214109 (2008).
[13] N. Bernstein, M. J. Aziz, and E. Kaxiras, Phys. Rev. B **61**, 6696 (2000).
[14] T. Motooka, K. Nisihira, S. Munetoh, K. Moriguchi, and A. Shintani, Phys. Rev. B **61**, 8537 (2000).
[15] K. Gärtner and B. Weber, Nucl. Instrum. Methods Phys. Res. B **202**, 255 (2003).
[16] A. Mattoni and L. Colombo, Phys. Rev. B **69**, 045204 (2004).
[17] C. Krzeminski, Q. Brulin, V. Cuny, E. Lecat, E. Lampin, and F. Cleri, J. Appl. Phys. **101**, 123506 (2007).
[18] F. H. Stillinger and T. A. Weber, Phys. Rev. B **31**, 5262 (1985).
[19] K. Ding and H. C. Andersen, Phys. Rev. B **34**, 6987 (1986).
[20] Zi Jian, Z. Kaiming, and X. Xide, Phys. Rev. B **41**, 12915 (1990).
[21] C. Roland and G. H. Gilmer, Phys. Rev. B **47**, 16286 (1993).
[22] M. Laradji, D. P. Landau, and B. Dünweg, Phys. Rev. B **51**, 4894 (1995).
[23] J. C. Noya, C. P. Herrero, and R. Ramirez, Phys. Rev. B **56**, 237 (1997).
[24] C. P. Herrero, J. Mater. Res. **16**, 2505 (2001).
[25] W. Yu, Z. Q. Wang, and D. Stroud, Phys. Rev. B **54**, 13946 (1996).
[26] Q. Yu and P. Clancy, J. Cryst. Growth **149**, 45 (1995).
[27] K. Nordlund, M. Ghaly, R. S. Averback, M. Caturla, T. Diaz de la Rubia, and J. Tarus, Phys. Rev. B **57**, 7556 (1998).
[28] Z. Q. Wang and D. Stroud, Phys. Rev. B **38**, 1384 (1988).
[29] J. Tersoff, Phys. Rev. B **39**, 5566 (1989).
[30] M. Posselt, F. Gao, and H. Bracht, Phys. Rev. B **78**, 035208 (2008).
[31] H. J. C. Berendsen, J. P. M. Postma, W. F. van Gunsteren, A. DiNola, and J. R. Haak, J. Chem. Phys. **81**, 3684 (1984).
[32] *CRC Handbook of Chemistry and Physics*, 87th ed., edited by D. R. Lide (CRC Press, Boca Raton, 2006).
[33] E. P. Donovan, F. Spaepen, D. Turnbull, J. M. Poate, and D. C. Jacobson, J. Appl. Phys. **57**, 1795 (1985).
[34] R. Hultgren, P. D. Desai, D. T. Hawkins, M. Gleiser, K. K. Kelly, and D. D. Wagman, *Selected Values of the Thermodynamical Properties of the Elements* (American Society for Metals, Metals Park, OH, 1973).
[35] J. R. Morris, C. Z. Wang, K. M. Ho, and C. T. Chan, Phys. Rev. B **49**, 3109 (1994).
[36] J. P. Gabathuler and S. Steeb, Z. Naturforsch. A **34A**, 1314 (1979).
[37] P. S. Salmon, J. Phys. F: Met. Phys. **18**, 2345 (1988).
[38] Y. Waseda and K. Suzuki, Z. Phys. B **20**, 339 (1975).
[39] A. Filipponi and A. Di Cicco, Phys. Rev. B **51**, 12322 (1995).
[40] W. D. Luedtke and U. Landman, Phys. Rev. B **37**, 4656 (1988).
[41] K. Laaziri, S. Roorda, and J. M. Baribeau, J. Non-Cryst. Solids **191**, 193 (1995).
[42] G. Petö, Z. F. Horváth, O. Gereben, L. Pusztai, F. Hajdú, and E. Sváb, Phys. Rev. B **50**, 539 (1994).
[43] R. J. Temkin, W. Paul, and G. A. N. Connell, Adv. Phys. **22**, 581 (1973).
[44] N. J. Shevchik and W. Paul, J. Non-Cryst. Solids **13**, 1 (1973); **8-10**, 381 (1972).
[45] G. Etherington, A. C. Wright, J. T. Wenzel, J. C. Dore, J. H. Clarke, and R. N. Sinclair, J. Non-Cryst. Solids **48**, 265 (1982).
[46] M. C. Ridgway, C. J. Glover, K. M. Yu, G. J. Foran, C. Clerc, J. L. Hansen, and A. Nylandsted Larsen, Phys. Rev. B **61**, 12586 (2000).
[47] J. Ankele, J. Mayer, P. Lamparter, and S. Steeb, J. Non-Cryst. Solids **192-193**, 679 (1995).
[48] F. Spaepen and D. Turnbull, AIP Conf. Proc. No. 50 (AIP, New York, 1979), p. 73.
[49] D. Klinger, J. Auleytner, and D. Zymierska, Cryst. Res. Technol. **32**, 983 (1997).
[50] *Pulsed Laser Processing of Semiconductors*, Semiconductors & Semimetals Vol. 23, edited by R. F. Wood, C. W. White, and R. T. Young (Academic Press, New York, 1984), p. 693.
[51] J. K. Bording, Phys. Rev. B **62**, 7103 (2000).
[52] G. Kresse and J. Hafner, Phys. Rev. B **49**, 14251 (1994).
[53] J. Chai, D. Stroud, J. Hafner, and G. Kresse, Phys. Rev. B **67**, 104205 (2003).
[54] L. A. Marques, M.-J. Caturla, T. Diaz de la Rubia, and G. H. Gilmer, J. Appl. Phys. **80**, 6160 (1996).
[55] J. S. Williams, in *Surface Modification and Alloying*, edited by J. M. Poate and G. Foti (Plenum Press, New York, 1983), pp. 133–163.
[56] J. M. Poate and J. S. Williams, *Ion Implantation and Beam Processing* (Academic Press, New York, 1984), pp. 13–57.
[57] K. L. Saenger, K. E. Fogel, J. A. Ott, D. K. Sadana, and H. Yin, J. Appl. Phys. **101**, 104908 (2007).
[58] J. Tersoff, Phys. Rev. B **38**, 9902 (1988).